IEEE Access
Multidisciplinary | Rapid Review | Open Access Journal

Received July 2, 2019, accepted July 22, 2019, date of publication July 29, 2019, date of current version August 12, 2019.

Digital Object Identifier 10.1109/ACCESS.2019.2931424

Research on Vibration Characteristics and Stress Analysis of Gearbox Housing in High-Speed Trains

HAO WU[1,2], PINGBO WU[1], KAI XU[2,3], JINCHENG LI[3], AND FANSONG LI[1]

[1]State Key Laboratory of Traction Power, Southwest Jiaotong University, Chengdu 610031, China
[2]Mechanical Science and Engineering, University of Illinois at Urbana–Champaign, Champaign, IL 61801, USA
[3]School of Mechanical Engineering, Southwest Jiaotong University, Chengdu 610031, China

Corresponding author: Fansong Li (lifansong2013@163.com)

This work was supported in part by the National Key Research and Development Program of China under Grant 2017YFB1201304-13, in part by the National Natural Science Foundation of China under Grant 11790282, and in part by the Fundamental Research Funds for the Central Universities under Grant 2682019CX47.

ABSTRACT Gearbox housing in high-speed trains has two kinds of excitation sources: the internal excitation of gear mesh excitation and the external excitation that contains the wheel polygonization and the input torque. To study the effect of the torque on the vibration and stress of the gearbox housing, a multibody dynamic model is established by the Simpack, in which the elastic deformation of the wheelset and the gearbox housing are considered. A traction drive system is modeled by the MATLAB/Simulink to calculate the traction torque, which is transformed to drive the high-speed train to overcome the basic resistance and run with a constant speed. The accuracy of the model is verified by comparing the simulation results with the measurement results. Based on the electromechanical model, the vibration acceleration of the gearbox housing in the case of without torque, with ideal torque, and with harmonic torque is calculated and analyzed, as well as its dynamic stress. The results show that the traction torque plays a role in amplifying the vibration acceleration and dynamic stress. When the fatigue damage of the gearbox housing is calculated, it will obtain a more accurate result to consider the effect of the traction torque.

INDEX TERMS Vehicle dynamics, traction motors, harmonic analysis, torque, acceleration, stress.

I. INTRODUCTION

Research on vibration and structural fatigue of vehicle components is an essential issue in the field of mechanical engineering, affecting the comfort and safety of vehicle operation [1], [2]. As a critical component to transmit traction power in the high-speed train, the gearbox is working at an environment with multiple inputs and strong coupling. The gear end of the gearbox is jointed to the wheelset axle with bearings, the pinion end is connected to the bogie frame by a C bracket, and the pinion shaft is coupled with the traction motor by a coupling. Therefore, wheel-rail contact and traction torque, which are both of external excitation, excite the vibration of the gearbox. The reliability of the gearbox directly affects the running safety of the high-speed train. Nowadays, mechanical products have paid more and more attention to the requirements of high reliability and long life [3], [4]. Hence, it has significant importance to study the vibration characteristics and stress analysis of the gearbox housing.

Hu *et al.* [5] analysis the measured dynamic stress of gearbox housing and shows that the wheel-rail impact excited the gearbox housing resonance modes. Dion *et al.* [6] analyzed the gear meshing impact phenomenon of the gearbox, and defined the intermeshing gear pair contact relationship as an elastic nonlinear topological contact model. The research focused on the gear meshing excitation inside the gearbox. Choy *et al.* [7] used the modal analysis method to decouple the equation of motion of the gearbox and convert it into independent modal equations, and calculated the dynamic characteristics of the gearbox box according to the structural features of the box and the gear transmission parameters. Huang *et al.* [8] established a dynamics model of a high-speed train and a finite element model of the gearbox housing, which were used to analyze the influence of internal and external excitations on the structure fatigue.

The associate editor coordinating the review of this manuscript and approving it for publication was Chong Leong Gan.

Moyne *et al.* [9] uses boundary finite element method and experimental method to evaluate the acoustic radiation of a gearbox housing, adding different types of stiffeners to the gearbox housing, and exploring the effect of different kinds of stiffeners on acoustic radiation.

As the published literature shows, there are many kinds of research that focus on the vibration characteristics of the gearbox, and also lots of literature [10], [11] concentrate on the influence of wheel-rail excitation on the gearbox housing, such as wheel polygonization [12], [13], which often occurs during the operation of high-speed trains. However, few of them considered the effect of traction torque on the gearbox housing. High-speed trains transmit traction torque to the gearbox through asynchronous motors, so motor torque is also an essential source of excitation for the gearbox.

Kang and Sul [14] proposed a direct torque control method of an induction machine which enables the minimum torque ripple control while maintaining constant switching frequency. Siami *et al.* [15] presents a modified predictive torque control for a permanent magnet synchronous motor to reduce the torque ripple at the presence of parametric uncertainty by improving the prediction accurateness. Most of the literature about motor torque focus on ripple reduction methods, which means that torque ripple is a severe problem in the transmission system.

In this paper, the gearbox housing on high-speed trains is taken as the main object to study its dynamic vibration characteristics and dynamic stress in the condition of wheel polygonization and traction torque. The remainder of this paper is organized as follows. The rigid-flexible dynamics model of the high-speed train is established in Section II, in which the gearbox housing and wheelset are considered as flexible bodies. The basic resistance of the high-speed train is calculated and applied to the carbody, the electrical traction control system is used to provide traction torque for motors to overcome the resistance. In Section III and Section IV, the dynamics model is driven by the ideal torque and the harmonic torque, respectively, to study the dynamic vibration response and fatigue damage of the gearbox housing. Section V concludes the paper.

II. ELECTROMECHANICAL COUPLING MODEL

A. MULTIBODY DYNAMICS MODEL

The model used in this paper refers to previous research [11], and a brief introduction is given in this paper. As a multibody dynamics model, it consists of a carbody, two bogie frames, four wheelsets, and four traction drive systems. The complicated relationships between these bodies are as shown in Figure 1. In the model, the gearbox housing and the wheelset are considered as flexible bodies, the detailed method to describe the flexible bodies in the multibody dynamic model refers to previous research [16]. The formula of the motion of the multibody system can be described as follows

$$[M]\{\ddot{x}\} + [C]\{\dot{x}\} + [K]\{x\} = \{F\} \tag{1}$$

where $[M]$, $[C]$, $[K]$ are the mass matrix, the damping matrix and the stiffness matrix of the multibody system respectively, $\{x\}$ is the displacement vector, $\{F\}$ is the vector of loads applied on the vehicle.

The wheel-rail contact force is determined by the Hertzian nonlinear contact theory as follows

$$f_j(t) = \begin{cases} \left\{\frac{1}{G}\delta Z_j(t)\right\}^{3/2} & \delta Z_j(t) > 0 \\ 0 & \delta Z_j(t) \le 0 \end{cases} \tag{2}$$

where G is the wheel/rail contact constant, and $\delta Z_j(t)$ is the elastic compression deformation of the jth wheelset and rail at the contact point in the normal direction, which is given as [17]

$$\delta Z_j(t) = Z_{wj}(t) - Z_r(x_j, t) - Z_{0j}(t)\ (j = 1 - 4) \tag{3}$$

where $Z_{wj}(t)$ is the displacement of the jth wheelset, $Z_r(x_j, t)$ is the rail displacement under the jth wheelset, $Z_{0j}(t)$ is the track irregularity under the jth wheelset.

The harmonic deviation is used preliminarily to describe the ideal polygonal wear in the wheel circumferential direction. The formulas are given as follows

$$\begin{cases} x = (R + AsinN\theta)sin\theta \\ y = (R + AsinN\theta)cos\theta \end{cases} \tag{4}$$

where R is the radius of wheel; A is the amplitude of polygonal wear; N is the order of wheel polygonization and θ is the wheel rotation angle.

According to the measured polygonal wear of 8 wheelsets by the ΦDS measurement instrument with the uncertainty of 0.05% as shown in Figure 2, it can be seen that 18-20th polygonal wear dominates in most of the railway wheelsets. The diameter of the wheel of the high-speed train in China is mostly between 800 mm and 920 mm. When the train is running at 300 km/h, a high-frequency excitation between 519 Hz-663 Hz will be caused by the 18-20th polygonal wheel. Thus, the 20th polygonal wear of wheel as shown in Figure 3 is considered in the calculation, which will causes the 578 Hz excitation resonance the gearbox housing based on the structure used in this paper.

B. TRACTION CHARACTERISTICS

Traction motors used on high-speed trains are mostly asynchronous traction motors, and their traction characteristics can be divided into two phases: constant torque and constant power. The traction force can be expressed as follows

$$F = \begin{cases} lv + m & v \le v_0 \\ \dfrac{P}{v} & v > v_0 \end{cases} \tag{5}$$

where F is traction force, v is running speed of the high-speed train, l and m are traction coefficient corresponding to vehicle model, and P is the rated power of the motor.

High-speed trains need to overcome the basic resistance generated by friction between the train surface and the air

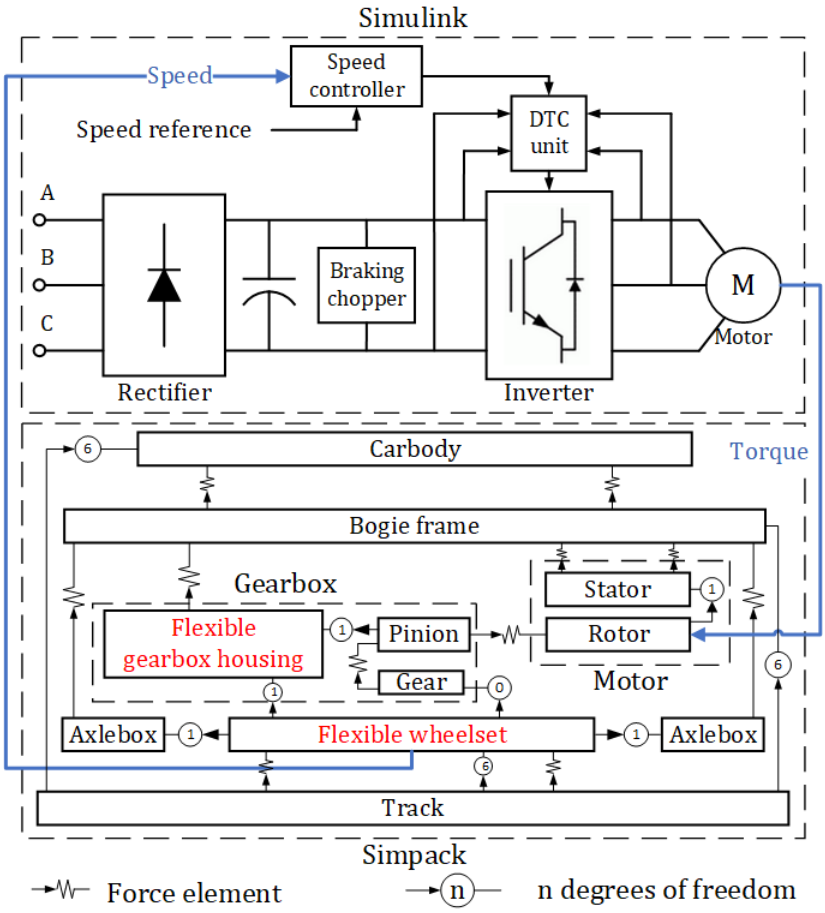

FIGURE 1. Electromechanical coupling model of the high-speed train.

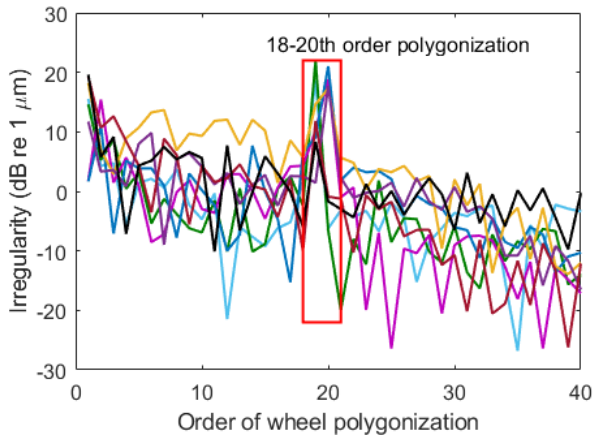

FIGURE 2. Measured irregularity spectrum of polygonization.

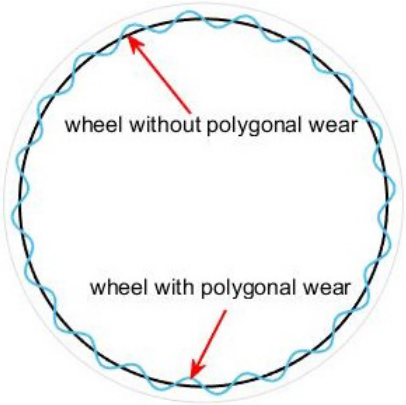

FIGURE 3. Wheel used in calculation.

as well as between the wheels and the rail during operation. It is difficult to accurately calculate the running resistance of high-speed trains through theoretical analysis. In practice, the basic resistance is usually estimated by tests, so that the basic resistance calculation formula for different models is as follows

$$W_0 = a + bv + cv^2 \tag{6}$$

where W_0 is basic resistance per ton of the high-speed train, a, b, c are coefficient corresponding to vehicle model.

C. TRACTION CONTROL SYSTEM

The high-speed train receives power through the pantograph and turns the 25kV single-phase AC power into the three-phase AC power via a transformer, a rectifier, a chopper, and

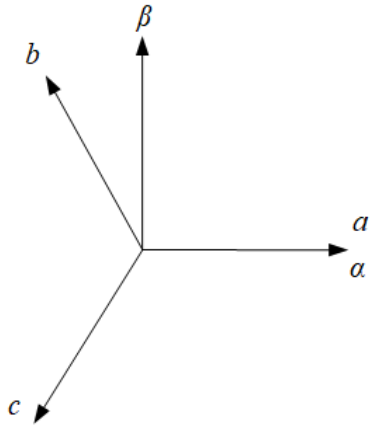

FIGURE 4. Clarke transformation.

an inverter. The whole process is an AC-DC-AC conversion process.

The asynchronous motor is a multi-input, multi-output, high-order, strong coupling and nonlinear multivariable system in a three-phase coordinate system. The Clarke transformation [18], as shown in Figure 4 is used to simplify the mathematical model and convert the three-phase coordinate system into a two-phase stationary coordinate system, to obtain a linear and decoupled mathematical model. The Clarke transformation can be expressed as

$$\begin{bmatrix} \alpha \\ \beta \end{bmatrix} = \sqrt{\frac{2}{3}} \begin{bmatrix} 1 & -\frac{1}{2} & -\frac{1}{2} \\ 0 & \frac{\sqrt{3}}{2} & -\frac{\sqrt{3}}{2} \end{bmatrix} \begin{bmatrix} a \\ b \\ c \end{bmatrix} \tag{7}$$

The mathematical model of the motor in a two-phase stationary coordinate system can be obtained by the Clarke transformation. The voltage equation of asynchronous traction motor in the two-phase stationary coordinate system is calculated

$$\begin{bmatrix} u_{s\alpha} \\ u_{s\beta} \\ u_{r\alpha} \\ u_{r\beta} \end{bmatrix} = \begin{bmatrix} R_s + L_s p & 0 & L_m p & 0 \\ 0 & R_s + L_s p & 0 & L_m p \\ L_m p & \omega_r L_m & R_r + L_r p & \omega_r L_r \\ -\omega_r L_m & L_m p & -\omega_r L_r & R_r + L_r p \end{bmatrix} \begin{bmatrix} i_{s\alpha} \\ i_{s\beta} \\ i_{r\alpha} \\ i_{r\beta} \end{bmatrix} \tag{8}$$

where $u_{s\alpha}$ and $u_{s\beta}$ are the components of the stator voltage on the α-axis and β-axis of the two-phase stationary coordinate system; $u_{r\alpha}$ and $u_{r\beta}$ are the components of the rotor voltage; $i_{s\alpha}$ and $i_{s\beta}$ are the components of the stator current; $i_{r\alpha}$ and $i_{r\beta}$ are the components of the rotor current; R_s is the stator resistance and R_r is the rotor resistance; Lm is the magnetizing reactance, L_s is the stator leakage reactance, L_r is the rotor leakage reactance referred to stator; p is the differential operator; ω_r is the rotor angular frequency.

Flux equation can be obtained as follows

$$\begin{bmatrix} \lambda_{s\alpha} \\ \lambda_{s\beta} \\ \lambda_{r\alpha} \\ \lambda_{r\beta} \end{bmatrix} = \begin{bmatrix} L_s & 0 & L_m & 0 \\ 0 & L_s & 0 & L_m \\ L_m & 0 & L_r & 0 \\ 0 & L_m & 0 & L_r \end{bmatrix} \begin{bmatrix} i_{s\alpha} \\ i_{s\beta} \\ i_{r\alpha} \\ i_{r\beta} \end{bmatrix} \tag{9}$$

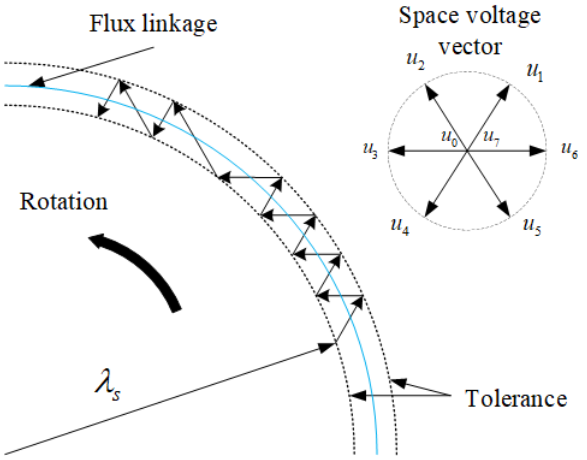

FIGURE 5. Stator flux linkage.

TABLE 1. Primary parameters of the traction motor.

Quantity	Conversion from Gaussian	Unit
Rated power	562	kW
Rated frequency	139	Hz
Rated stator voltage	2700	V
Rated speed	4100	r/min
Number of pole pairs	2	
Stator resistance	0.15	Ω
Stator inductance	1.42	mH
Rotor resistance	0.16	Ω
Rotor inductance	0.6	mH
Magnetizing inductance	25.4	mH
Moment of inertia	5	kg·m^2
Stator flux	1.7	Wb
Flux tolerance	0.025	Wb

where $\lambda_{s\alpha}$ and $\lambda_{s\beta}$ are the components of the stator flux linkage in the α-axis and β-axis of the two-phase stationary coordinate system; $\lambda_{r\alpha}$ and $\lambda_{r\beta}$are the components of the rotor flux linkage.

In this paper, the amplitude of the stator flux linkage is controlled to maintain stability based on the direct torque control (DTC) algorithm [19] to ensure the rapidity of the system. According to (8) and (9), the stator voltage and current frequency determine the flux linkage size when neglecting the influence of stator resistance as follows

$$\lambda_s^{t+\Delta t} = \int (u_s - i_s R_s)\, dt \approx u_s \cdot \Delta t + \lambda_s^t \tag{10}$$

A two-level inverter can generate eight kinds of space voltage vectors, as shown in Figure 5. The inverter generates the required space voltage vector under the action of the switching command output by the DTC controller to ensure that the stator flux linkage is within a given flux tolerance.

The electromechanical coupling model of the high-speed train is established as shown in Figure 1. The traction control system is modeled in MATLAB/Simulink, and the multibody dynamic system is modeled in Simpack. The sample frequency is set to 5000 Hz and SIMAT file in Simpack is used to coupling the two software. Primary parameters of the traction motor are given as Table 1.

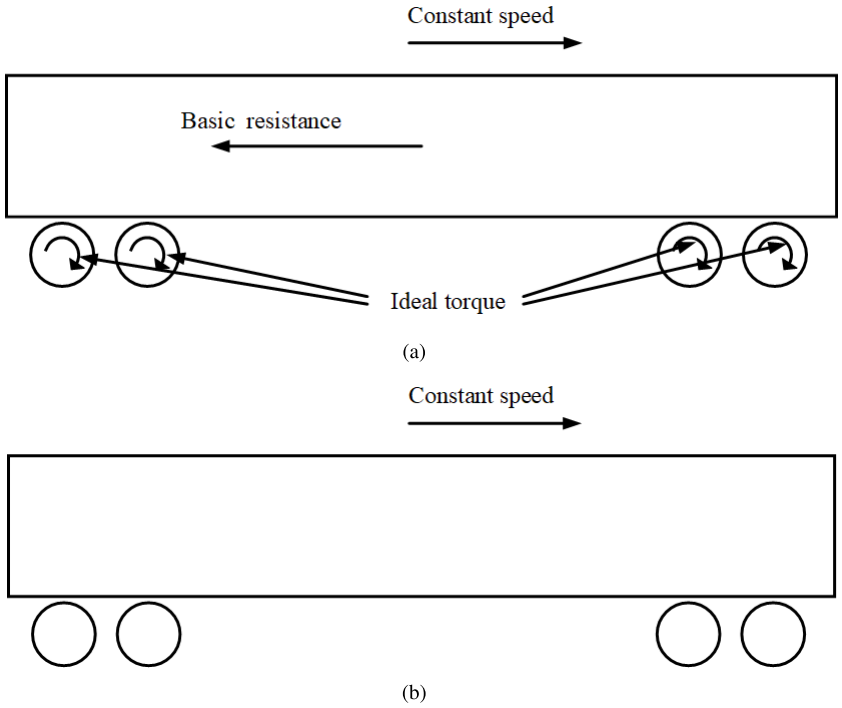

FIGURE 6. Cases of (a) running with ideal torque (b) running without torque.

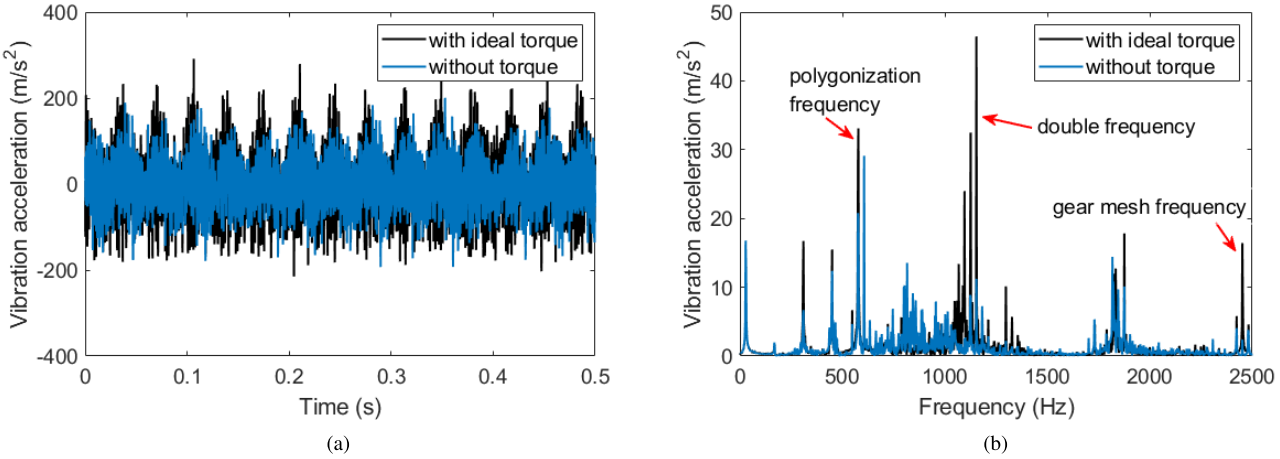

FIGURE 7. Vibration of the gearbox housing in (a) time domain (b) frequency spectrum.

III. STUDY ON IDEAL TORQUE

A. VIBRATION CHARACTERISTICS

In this section, the traction drive system is simplified as an ideal system. The motor is directly driven by an ideal three-phase sinusoidal voltage, which means the torque ripple is neglected. The two operating cases shown in Figure 6 are considered: one is that the high-speed train operates at a uniform speed against the basic resistance when the motor outputs the ideal torque as shown in Figure 6(a), and the other is shown in Figure 6(b) that the train runs at a constant speed without torque and without resistance.

The dynamic response of the gearbox housing is calculated for the high-speed trains under these two conditions at a running speed of 300 km/h. The excitation of the track irregularity is neglected in the calculation for the reason that the eigen frequencies of the gearbox housing are far away from the excitation frequency of track irregularity, and only the excitation of the wheel polygonization is considered.

The time domain diagram and frequency spectrum of the vertical vibration acceleration of the gearbox housing are shown in Fig. 7(a) and Fig. 7(b). It can be seen from the time domain diagram that the vertical vibration acceleration amplitude of the gearbox housing in the case of with ideal torque reaches 300 m/s^2, in contrast, it is only 200 m/s^2 in the case of without torque. The frequency domain diagram shows that the vertical vibration acceleration of the gearbox housing

in the two cases has the following frequency components: 28 Hz which is the wheelset rotation frequency caused by the elastic deformation of the wheelset, 578 Hz which is the wheel polygonization excitation frequency and its double frequency of 1156 Hz, as well as 2450 Hz the gear mesh frequency.

Comparing the spectrograms of the two operating cases, it can be found that the amplitudes of the vibration components in the case of with ideal torque is 33 m/s^2 at 578 Hz, 46 m/s^2 at 1156 Hz, and 17 m/s^2 at 2450 Hz. Compare them to the case of without torque in which these amplitudes are 21 m/s^2 at 578 Hz, 11 m/s^2 at 1156 Hz and 2 m/s^2 at 2450 Hz, respectively. Through the above analysis, it can be known that when the high-speed train is running with torque, the motor torque plays a role in amplifying the vibration amplitude of the gearbox housing.

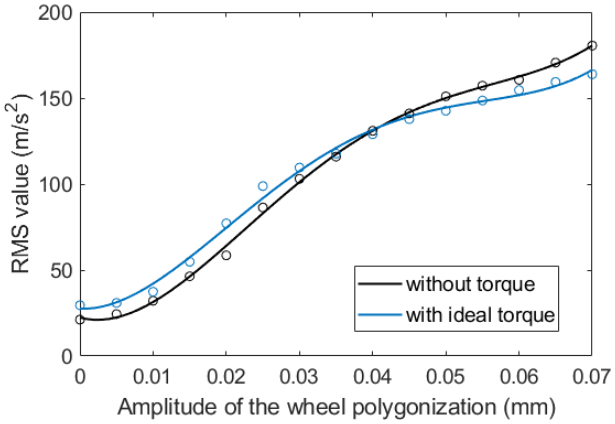

FIGURE 8. RMS value of the vibration acceleration in the cases of without torque and with ideal torque.

In this paper, the dynamic response of the gearbox housing is calculated when the wheel polygonization amplitude is in the range of 0 mm to 0.07 mm. By taking the root mean square (RMS) value of the vertical vibration acceleration of the gearbox housing, relationships between the RMS values and the amplitude of the wheel polygonization in the two operating conditions are shown in Fig. 8 respectively. It can be seen in the range of 0 mm to 0.04 mm that the RMS value of the vibration acceleration of the gearbox housing with ideal torque condition is larger than that without torque condition, as opposed to in the range of 0.04 mm to 0.07 mm, in which the RMS value in the case of with ideal torque is smaller than that without torque. The difference between the two shows an increasing trend as the amplitude of the wheel polygonization increases. FFT analysis is carried out on the vibration acceleration of the gearbox housing, and the vibration amplitudes at the wheel polygonization excitation frequency in the two operating conditions are shown in Fig. 9. The amplitude with ideal torque condition is 1.34 times as large as that without torque, which indicates that the torque excitation amplifies the vibration response of the gearbox housing with the wheel polygonization.

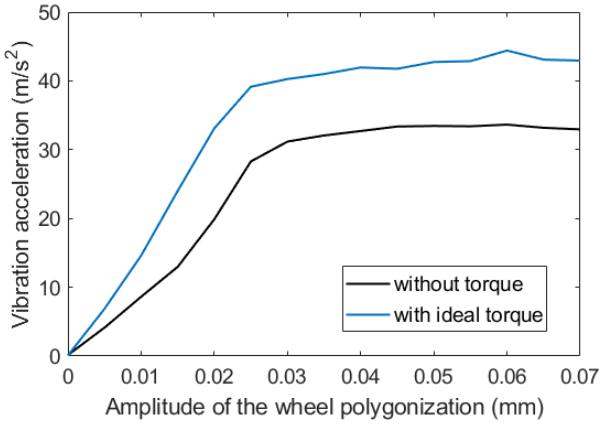

FIGURE 9. Amplitude of vibration component at 578 Hz in the cases of without torque and with ideal torque.

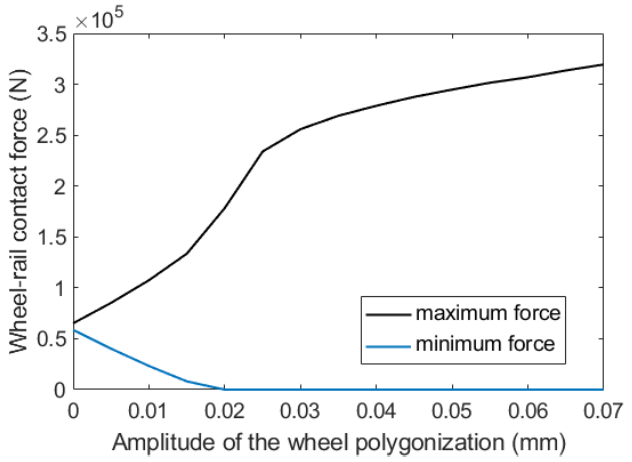

FIGURE 10. Wheel rail contact force.

Fig. 10 shows the minimum and maximum values of wheel-rail contact force, compare it to Fig. 8, it can be concluded that the RMS value trend of the gearbox housing vibration is consistent with the maximum trend of the wheel-rail contact force, and the curvature of both increases first and then decreases. When the wheel polygonization amplitude increases to 0.02 mm, the minimum wheel-rail contact force decreases to 0 N, indicating that the wheel is disengaged from the track. It can be seen from Fig. 8 that the RMS value in the case of without torque increases more than in the case of with ideal torque. The RMS value in the case of without torque exceeds that in the case of with ideal torque when the wheel polygonization amplitude reaches 0.04 mm.

Herein, the vertical vibration acceleration of a high-speed train gearbox housing between two stations is tested. The short-time Fourier transform analysis of the data is shown in Fig.11. It can be seen that during the constant speed operation of the high-speed train, the gearbox housing has a significant 578 Hz wheel polygonization frequency and its double frequency, as well as a gear mesh frequency of 2450 Hz. The dynamic model established in this paper has the same spectral composition as the actual structure, which can reflect

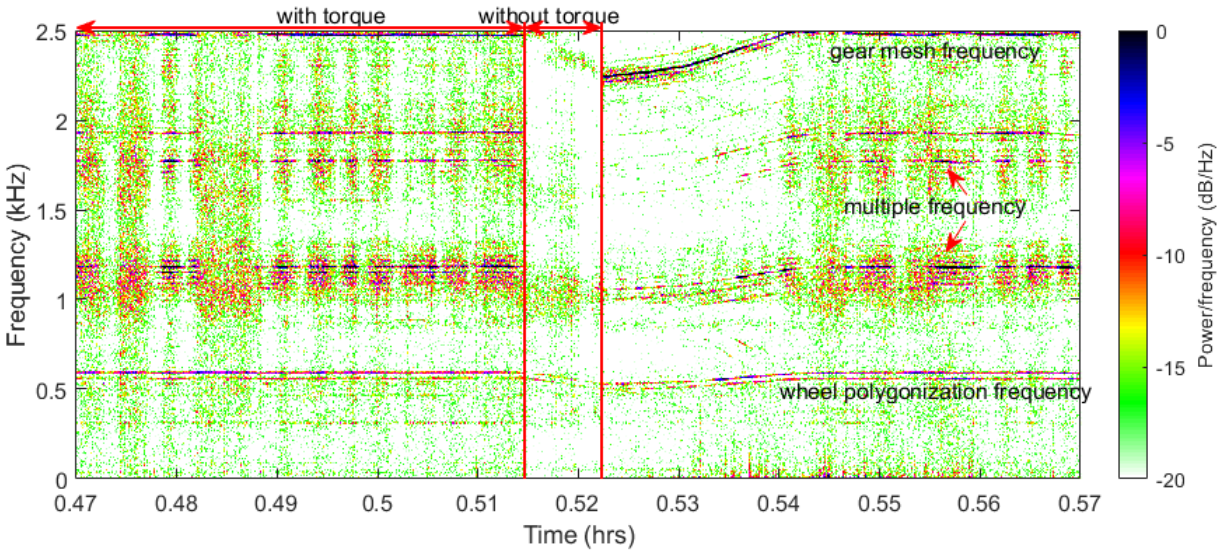

FIGURE 11. Short-time Fourier transform.

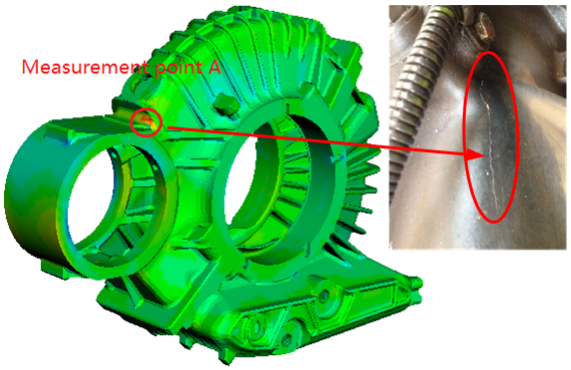

FIGURE 12. Stress distribution.

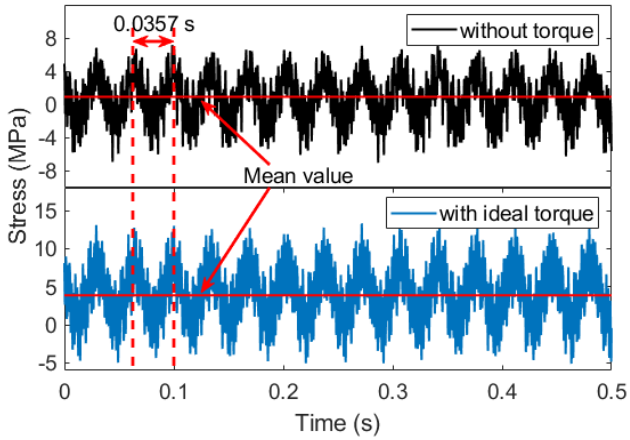

FIGURE 13. Stress of the measurement point A in the cases of without torque and with ideal torque.

the dynamic response of the high-speed train gearbox housing in actual operation. When the high-speed train runs through the neutral zone, it is in the inertial motion state. At this time, the vehicle has only the resistance and no traction torque. Fig.11 shows that the amplitude of each frequency component is significantly reduced in the neutral zone, which is consistent with the previous simulation results.

B. STRESS ANALYSIS

To study the effect of motor torque on the dynamic stress of the gearbox housing, in this section, the dynamic stress of the gearbox housing is calculated in two cases, with ideal torque, and without torque. The dynamic stress distribution of the gearbox housing is as shown in Fig. 12, it can be seen that the max stress occurs in a position nears to the inspection window corner, which is consistent with the cracking position of the actual structure.

Fig. 13 shows the dynamic stress of the measurement point A located in the position where the max stress occurs. It can be seen that the waveform of the dynamic stress in two conditions both show a shape of the sinusoidal wave with a period of 0.0357 s, which is the period of wheelset rotation. However, some differences between the two cases can be concluded: in the case of with ideal torque, the mean value of the gearbox housing stress is 3.87 MPa, and the amplitude of the stress is frustrate in the range of −5.11 MPa to 13.3 MPa. On the contrary, the mean value of the stress is 0.94 MPa and the stress range is from −7.01 MPa to 7.33 MPa in the case of without torque.

Fig. 14 shows the rainflow-counting results of the dynamic stress of the gearbox housing in the case of with ideal torque and without torque. It can be seen that the trend in the case of with ideal torque is similar to in the case of without torque, except that the amplitude in the case of with ideal torque is 0.28 times larger than that in the case of without torque in the same cycle.

IV. STUDY ON RIPPLE TORQUE

A. VIBRATION CHARACTERISTICS

From the analysis in Section III, it can be seen that considering the motor torque during simulation will aggravate the

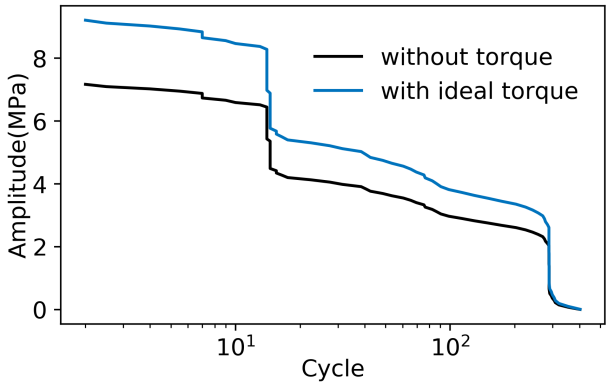

FIGURE 14. Rainflow-counting in the cases of without torque and with ideal torque.

vibration of the gearbox housing. The motor output in the actual operation is not the ideal torque, which contains the high-frequency harmonic components. According to the theory of AC motor speed regulation, the torque mainly includes the 6n (n=1, 2, 3,..) harmonic of the fundamental frequency. Therefore, in this section, the gearbox housing in the ideal torque condition and harmonic torque condition, as shown in Fig. 15 are analyzed and compared.

Using the traction control system established in Section II to carry out simulation calculation, the motor output torque is obtained as shown in Fig. 16(a). It can be seen from the figure that when the vehicle is running at a constant speed, the motor torque fluctuates up and down at the ideal torque value, and the fluctuation range is from 400 Nm to 1000 Nm. The spectrum analysis is shown in Fig. 16(b). It can be seen that 6X harmonic accounts for 3.7% of the fundamental wave, 12X harmonic accounts for 2.5% of the fundamental wave, and 18X harmonic accounts for 1.9% of the fundamental wave.

Fig. 17(a) shows that the vertical vibration acceleration of the gearbox housing with ideal torque and harmonic torque, and Fig. 17(b) shows the frequency spectrum. From the time domain diagram and the spectrum, there is little difference between the two conditions. Hence, the RMS values and the vibration component at 578 Hz are calculated under the amplitude of the wheel polygonization in the range of 0 mm to 0.07 mm. Fig. 18 shows that the RMS value in the condition with harmonic torque is slightly larger than that with ideal torque, and Fig. 19 shows that the amplitude of the vibration component at 578 Hz with harmonic torque is larger than that with ideal torque, and the larger the amplitude of the wheel polygonization, the larger the difference between the two conditions.

B. STRESS ANALYSIS

To study the effect of the harmonic torque on the dynamic stress of the gearbox housing, herein, the dynamic stress of the measurement point A also calculated in the case of with harmonic torque.

Fig. 20 shows the dynamic stress of the measurement point A. It can be seen that the waveform of the dynamic stress in two conditions both show the shape of the sinusoidal wave with a period of 0.0357 s. furthermore, differences

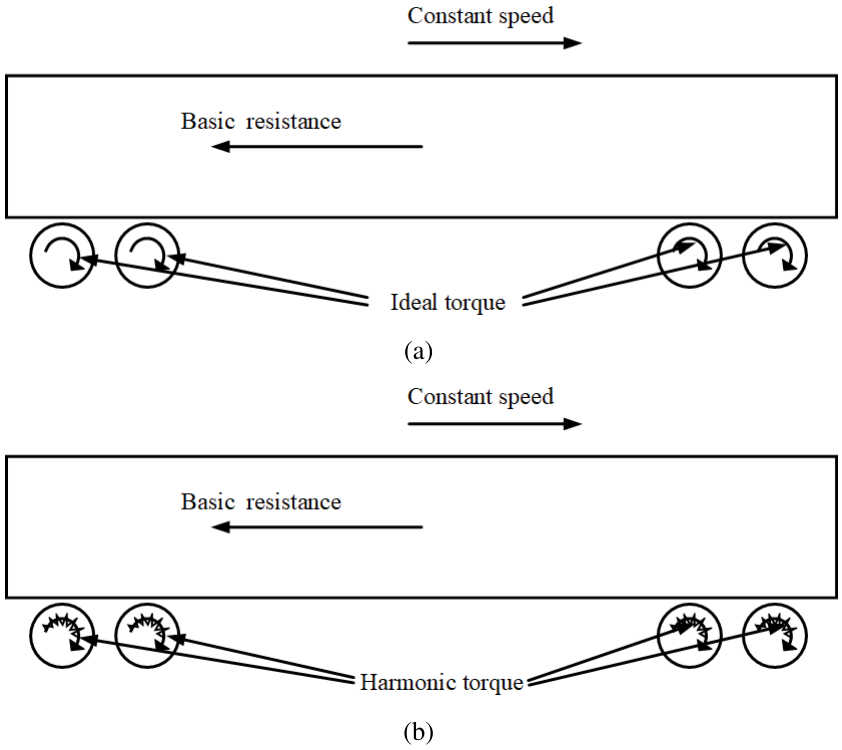

FIGURE 15. Cases of (a) running with ideal torque (b) running with harmonic torque.

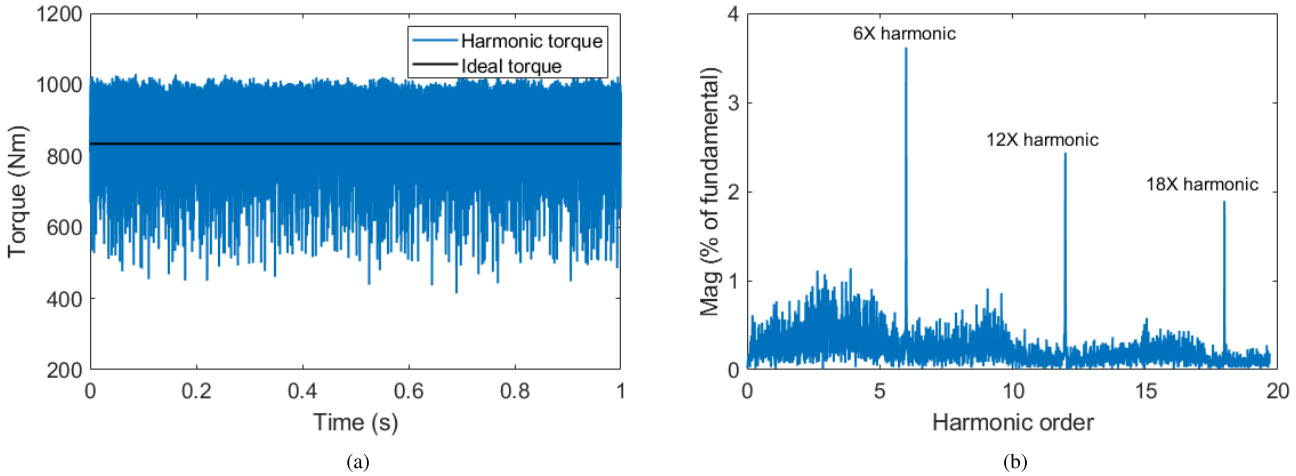

(a) (b)

FIGURE 16. Harmonic torque in (a) time domain (b) frequency spectrum.

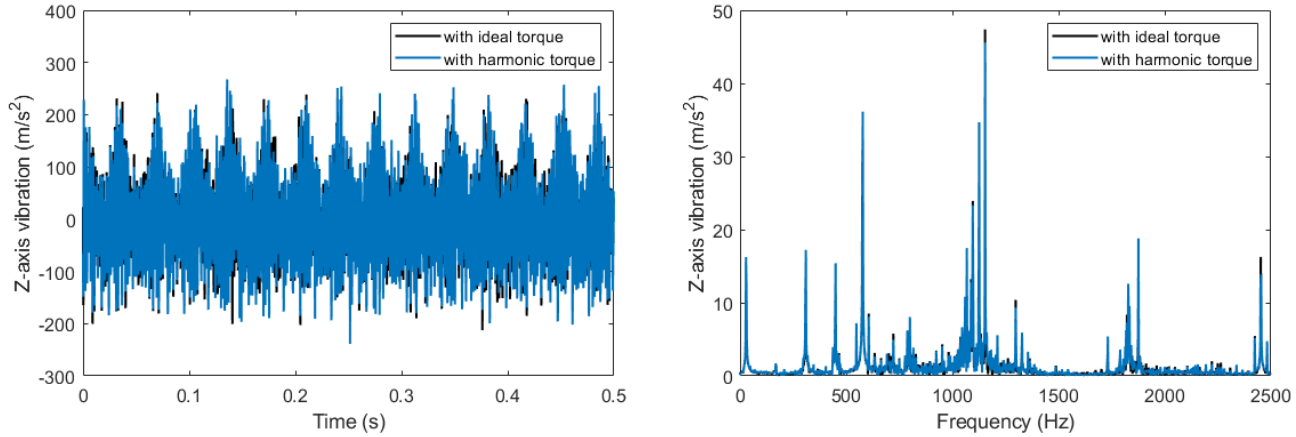

(a) (b)

FIGURE 17. Vibration acceleration in (a) time domain (b) frequency spectrum.

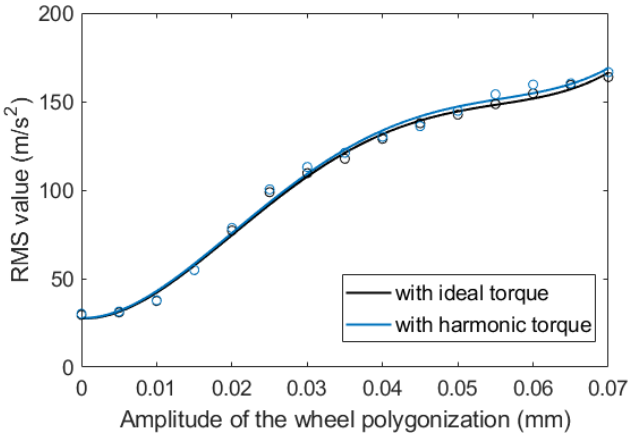

FIGURE 18. RMS value of the vibration acceleration in the cases of with ideal torque and with harmonic torque.

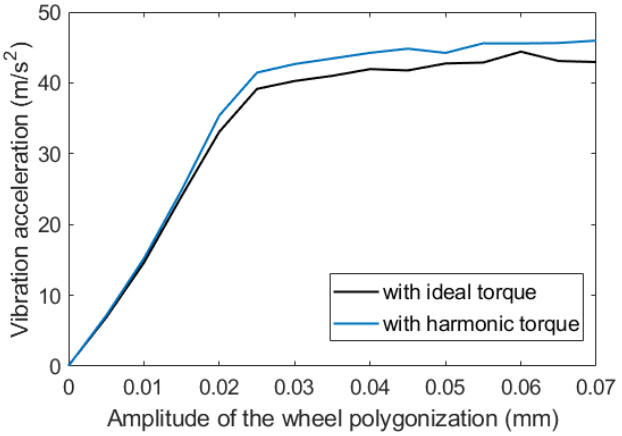

FIGURE 19. Amplitude of vibration component at 578 Hz in the cases of with ideal torque and with harmonic torque.

between the two conditions can be concluded: in the case of with harmonic torque, the mean value of the gearbox housing stress is 4.02 MPa, and the amplitude of the stress is frustrate in the range of −5.02 MPa to 13.8 MPa. On the contrary, the mean value of the stress is 3.87 MPa and the stress range is from −5.11 MPa to 13.3 MPa in the case of with ideal torque.

Fig. 21 shows the rainflow-counting results of the dynamic stress of the gearbox housing in the case of with harmonic

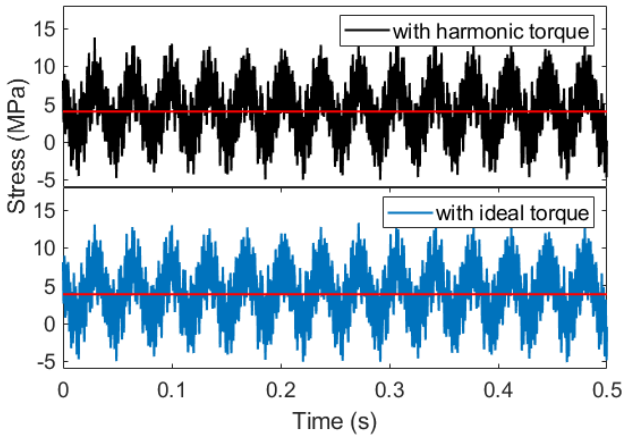

FIGURE 20. Stress of the measurement point A in the cases of with ideal torque and with harmonic torque.

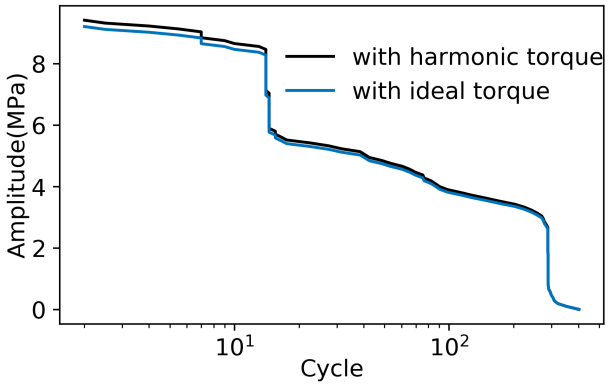

FIGURE 21. Rainflow-counting in the cases of with ideal torque and with harmonic torque.

torque and with ideal torque. It can be seen that the trend in the case of with ideal torque is similar to in the case of without torque, and the amplitude in the case of with harmonic torque is 0.02 times larger than in the case of with ideal torque in the same cycle.

V. CONCLUSION

This paper establishes a multi-body system dynamics model and a traction electric drive system model for high-speed trains, taking into account the elastic deformation of the gearbox housing and wheelset. The accuracy of the model is verified by comparing the simulation results with the measurement results. Study the vibration characteristics and dynamic stress characteristics of the gearbox housing in the cases of without torque, with ideal torque and with harmonic torque. Based on the above analysis, the following conclusions can be drawn:

In the case of with ideal torque, the amplitude of the vibration components at wheel polygonization frequency and its double frequency are both larger than in the case of without torque, as well as at the gear mesh frequency. It means that the ideal torque plays a role in amplifying these vibration components.

In the case of with ideal torque, the RMS value of vibration is larger than in the case of without torque when the amplitude of the wheel polygonization in the range of 0 mm to 0.04 mm, as opposed to in the range of 0.04 mm to 0.07 mm. However, the RMS value in the case of without torque increases more than in the case of with ideal torque when the wheel polygonization amplitude beyond 0.02 mm, and exceeds it when the amplitude beyond 0.04 mm. It can be concluded that the traction torque amplifies the vibration of the transmission housing when the wheel and track remain in contact, but attenuates the vibration when the wheel is disengaged from the rail.

The mean value of the dynamic stress and its frustration range are both increases in the case of with ideal torque when compare with the case of without torque, and the harmonic torque also has a slight influence on increasing the dynamic stress of the gearbox housing. It should be mentioned that the actual traction torque may contain much worse harmonic torque. When calculated the fatigue damage of the gearbox housing, it will obtain a more accurate result to consider the effect of the actual traction torque.

REFERENCES

[1] G. Sheng, *Vehicle Noise, vibration, and Sound Quality*. Warrendale, PA, USA: SAE, 2012.
[2] D. Wang, K.-L. Tsui, and Q. Miao, "Prognostics and health management: A review of vibration based bearing and gear health indicators," *IEEE Access*, vol. 6, pp. 665–676, 2018.
[3] J. Guo, Y.-F. Li, B. Zheng, and H.-Z. Huang, "Bayesian degradation assessment of CNC machine tools considering unit non-homogeneity," *J. Mech. Sci. Technol.*, vol. 32, no. 6, pp. 2479–2485, 2018.
[4] J. Guo, G.-Z. Fu, H.-Z. Huang, Y. Liu, and Y.-F. Li, "Characterizing wafer stage transmission errors via binary decision diagram and dynamic fault tree," *J. Mech. Sci. Technol.*, vol. 32, no. 11, pp. 5111–5119, 2018.
[5] W. Hu, Z. Liu, D. Liu, and X. Hai, "Fatigue failure analysis of high speed train gearbox housings," *Eng. Failure Anal.*, vol. 73, pp. 57–71, Mar. 2017.
[6] J. L. Dion, S. L. Moyne, G. Chevallier, and H. Sebbah, "Gear impacts and idle gear noise: Experimental study and non-linear dynamic model," *Mech. Syst. Signal Process.*, vol. 23, no. 8, pp. 2608–2628, Nov. 2009.
[7] F. K. Choy, Y. Ruan, R. Tu, J. J. Zakrajsek, and D. P. Townsend, "Modal analysis of multistage gear systems coupled with gearbox vibrations," *J. Mech. Des.*, vol. 114, no. 3, pp. 486–497, 1992.
[8] G.-H. Huang, N. Zhou, and W.-H. Zhang, "Effect of internal dynamic excitation of the traction system on the dynamic behavior of a high-speed train," *Proc. Inst. Mech. Eng. F, J. Rail Rapid Transit*, vol. 230, no. 8, pp. 1899–1907, 2016.
[9] S. Le Moyne, J. Tebec, and J.-C. Kraemer, "Source effect of ribs in sound radiation of stiffened plates. Experimental and calculation investigation," *Acta Acustica united with Acustica*, vol. 86, no. 3, pp. 457–464, 2000.
[10] Z. Wang, Y. Cheng, G. Mei, W. Zhang, G. Huang, and Z. Yin, "Torsional vibration analysis of the gear transmission system of high-speed trains with wheel defects," *Proc. Inst. Mech. Eng. F, J. Rail Rapid Transit*, to be published.
[11] H. Wu, P. Wu, F. Li, H. Shi, and K. Xu, "Fatigue analysis of the gearbox housing in high-speed trains under wheel polygonization using a multibody dynamics algorithm," *Eng. Failure Anal.*, vol. 100, pp. 351–364, Jun. 2019.
[12] E. Brommundt, "A simple mechanism for the polygonalization of railway wheels by wear," *Mech. Res. Commun.*, vol. 24, no. 4, pp. 435–442, 1997.
[13] M. Meywerk, "Polygonalization of railway wheels," *Arch. Appl. Mech.*, vol. 69, no. 2, pp. 105–120, 1999.
[14] J.-K. Kang and S.-K. Sul, "New direct torque control of induction motor for minimum torque ripple and constant switching frequency," *IEEE Trans. Ind. Appl.*, vol. 35, no. 5, pp. 1076–1082, Sep. 1999.
[15] M. Siami, D. A. Khaburi, and J. Rodíguez, "Torque ripple reduction of predictive torque control for PMSM drives with parameter mismatch," *IEEE Trans. Power Electron.*, vol. 32, no. 9, pp. 7160–7168, Sep. 2017.

[16] H. Shi and P. Wu, "Flexible vibration analysis for car body of high-speed EMU," *J. Mech. Sci. Technol.*, vol. 30, no. 1, pp. 55–66, Jan. 2016.
[17] Y. Sun, Y. Guo, Z. Chen, and W. Zhai, "Effect of differential ballast settlement on dynamic response of vehicle–track coupled systems," *Int. J. Struct. Stability Dyn.*, vol. 18, no. 7, pp. 1850091-1–1850091-29, 2018.
[18] S. Chattopadhyay, M. Mitra, and S. Sengupta, "Area based approach for three phase power quality assessment in clarke plane," *J. Elect. Syst.*, vol. 4, no. 1, pp. 60–76, 2008.
[19] B. K. Bose, *Modern Power Electronics and AC Drives*, vol. 123. Upper Saddle River, NJ, USA: Prentice-Hall, 2002.

HAO WU received the B.S. and M.S. degrees from Southwest Jiaotong University, China, in 2012 and 2015, respectively, where he is currently pursuing the Ph.D. degree. He is currently with the University of Illinois at Urbana–Champaign as a Visiting Scholar. His research interest includes failure mechanism of transmission system in high-speed trains.

PINGBO WU received the B.S., M.S., and Ph.D. degrees from Southwest Jiaotong University, China, in 1990, 1993, and 1997, respectively, where he is currently a Professor with the State Key Laboratory of Traction Power. His research interests include vehicle dynamics and structure fatigue.

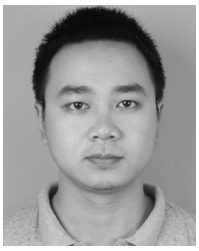

KAI XU received the B.S. and M.S. degrees from Southwest Jiaotong University, China, in 2011 and 2015, respectively, where he is currently pursuing the Ph.D. degree. He was with the University of Illinois at Urbana–Champaign, as a Visiting Scholar, in 2018. His research interests include dynamics and wheel wear in high-speed trains.

JINCHENG LI received the B.S. degree from Southwest Jiaotong University, China, in 2014, where he is currently pursuing the Ph.D. degree. His research interest includes the dynamic behavior of high-speed trains in railway turnout.

FANSONG LI received the B.S. and Ph.D. degrees from Southwest Jiaotong University, China, in 2012 and 2017, respectively, where he is currently an Assistant Professor with the State Key Laboratory of Traction Power. His research interests include vehicle dynamics and structure fatigue.